

Chapter 5

Surface-Wave Enhanced Biosensing

**Wolfgang Knoll,^{a,b} Amal Kasry,^a Chun-Jen Huang,^c Yi Wang,^b
and Jakub Dostalek^{a,b}**

^a*AIT Austrian Institute of Technology, Vienna, Austria*

^b*Center for Biomimetic Sensor Science,
School of Materials Science and Engineering,
Nanyang Technological University, Singapore*

^c*Graduate Institute of BioMedical Engineering,
National Central University, Jhongli City, Taiwan*

jakub.dostalek@ait.ac.at

5.1 Introduction

In 1983, a seminal paper by Bo Liedberg et al. introduced the first concept for the use of a particular type of surface waves, surface plasmon polaritons or surface plasmons for short, for biosensing [1]. Shortly thereafter, the first commercial implementation of surface plasmon resonance (SPR) spectroscopy for the detection of bioaffinity reactions appeared on the market [2]. Now, 30 years later, we look back to a remarkable success of this concept with numerous instruments being commercially available and a variety of modifications and extensions of the original principle being developed and described in the literature [3].

Introduction to Plasmonics: Advances and Applications

Edited by Sabine Szunerits and Rabah Boukherroub

Copyright © 2015 Pan Stanford Publishing Pte. Ltd.

ISBN 978-981-4613-12-5 (Hardcover), 978-981-4613-13-2 (eBook)

www.panstanford.com

Our own contribution to the further extension of SPR in biosensing concerns mostly four different directions: (i) the introduction of the concept of surface plasmon modes as surface light that is bound to an interface between a (noble) metal and a dielectric medium but otherwise interacts with matter in a way totally equivalent to plane waves [4]. This allowed, e.g., for the introduction of the surface plasmon diffraction mode for biosensing [5–7], or for the development of surface plasmon microscopy [8–10]. (ii) The second extension was the combination of the field-enhancement associated with resonant excitation of surface plasmons and the principles of fluorescence detection [11, 12]. This allowed us to amplify fluorescence signal strength and extend the limit of detection (LOD) into the attomolar range [13], an analyte concentration regime that was and still is not accessible for a label-free detection mode. A few principles and examples of this surface plasmon fluorescence spectroscopy for the use in bioaffinity detection are summarized in Section 5.2. (iii) As introduced by D. Sarid in the early 1980s [14], if two surface plasmon modes travelling along (nearly) identical metal/dielectric interfaces interact by coupling their optical fields, e.g., through a metallic layer thinner than twice the decay length of the plasmon field inside the metal, i.e., in the range of a few 10 nm, two new Eigen modes appear: the long-range surface plasmon (LRSP) and the short-range surface plasmon (SRSP). We extended this concept for biosensor studies by coupling again the specific features of the optical field enhancements of LRSP with fluorescence detection principles demonstrating that this way a significant enhancement of the already attractive limit of detection can be achieved [15, 16]. This will be briefly summarized in Section 5.3. (iv) And finally, we extended the concept of evanescent wave sensor platforms to other guided optical modes, in particular, to the various waveguide modes that can be excited in the identical (Kretschmann) setup if a thin dielectric layer in the range of a few 100 nm to several microns is deposited onto the surface plasmon guiding metal surface [17]. In Section 5.4, we demonstrate this for the use of hydrogels as the wave-guiding layer [18]. These interfacial architectures can be designed such as to act as the guiding material, serve as the sensor matrix layer with the immobilized recognition

sites, e.g., chemically attached antibodies [19], yet allow for the (nearly) unperturbed penetration of the analyte molecules by diffusion from the adjacent solution to the detection sites [20, 21].

5.2 Surface Plasmon Field-Enhanced Fluorescence Detection

One of the key principles for the design of surface sensor platforms is the correlation of the penetration length of the probing field, e.g., the decay of the shear field in the quartz crystal microbalance or the extend of the localized surface plasmon field for Au nanoparticles of different size with (the thickness of) the binding matrix of the sensor. For propagating surface plasmon modes (and in this short review we focus on these exclusively), the evanescent character of a surface plasmon mode manifests itself by an exponentially decaying optical field. The decay length into the metal is only a few or several 10 nm owing to the strong shielding effect of the nearly free electron gas in the metal; the decay length into the dielectric medium $L_p/2$ (where the bio-affinity reactions of interest happen) depends on (the complex) refractive index of the metal n_m , the employed laser wavelength, but also on the optical properties of the dielectric medium [4]. For the situation with a 50 nm thin Au layer in contact with water the (simulated) situation is shown in Fig. 5.1a: The evanescent field for a laser wavelength of $\lambda = 632.8$ nm reaches about $L_p/2 = 90$ nm into the aqueous phase (the decay length L_p is defined as a distance from a metal surface at which the field amplitude drops by a factor $1/e$). Correspondingly, the binding matrix used in the commercial chip CM5 from Biacore, a carboxymethylated dextran polymer brush, extends in the swollen state some 100–150 nm out into the buffer medium, thus matching the range that is probed by the optical surface plasmon field to the “slice” of the analyte solution with the bound species of interest (cf. Fig. 5.1b). This way, the number of binding events that can be probed by the optical sensor is considerably higher (by a factor of 3–5) than for a mere monomolecular arrangement of proteins bound directly to the transducer surface.

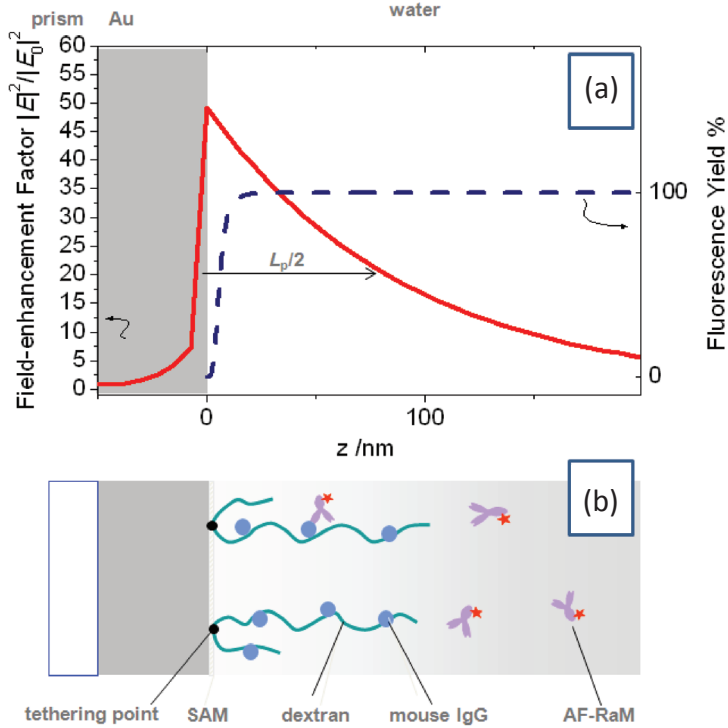


Figure 5.1 (a) Simulation of the spatial distribution normal to the interface of the optical field at resonant excitation of a surface plasmon mode between the thin Au layer as the metal and water as the dielectric medium; the peak intensity is located right at the interface, decaying quickly into the metal but also into the dielectric with a decay length of $L_p/2 = 90$ nm (for a laser wavelength of $\lambda = 632.8$ nm and Au refractive index $n = 0.125 + 3.56i$). For comparison, the dashed curve is a simulation of the fluorescence yield for a chromophore positioned at different distances away from the quenching metal layer. Only in the immediate proximity of the metal (up to a distance of about two Förster radii of 10–15 nm) a significant loss of fluorescence yield will lead to a reduced photon emission in surface plasmon fluorescence spectroscopy. (b) Schematics of a polymer brush (roughly to scale to the optical evanescent field in [a]) grafted to the sensor surface and functionalized by covalently attached antigens. To these binding sites chromophore-labeled antibodies can bind, still in the range of the resonantly enhanced optical field but outside the range of efficient fluorescence quenching.

Such a brush architecture as the binding matrix for the affinity reactions is also very beneficial for the fluorescence studies that we focus on in the following sections. As is also shown in Fig. 5.1a, the fluorescence yield of a chromophore near a metal surface that acts as a broadband acceptor system would be efficiently quenched for any bound (and labeled) analyte molecule that comes closer to the metal surface than about two Förster radii which amount to some 10–15 nm (cf. by the dashed curve in Fig. 5.1a) [22]. Any binding event that happens further away from that surface along the binding sites, e.g., chromophore-labeled antibodies binding to antigens that are covalently immobilized along the arms of the polymer brush (as sketched in Fig. 5.1b) results in a contribution to the fluorescence signal that is by no means weaker than from a free chromophore in solution. However, the evanescent character of the probing optical field with its finite decay length then limits the detected signal to the analyte molecules within the brush layer and, hence, is not overwhelmed by the abundance of analyte molecules in solution.

The experimental realization of a surface plasmon fluorescence spectrometer is schematically depicted in Fig. 5.2. Shown is an extension of a classical SPR spectrometer in the Kretschmann configuration with a coupling prism that matches the energy and

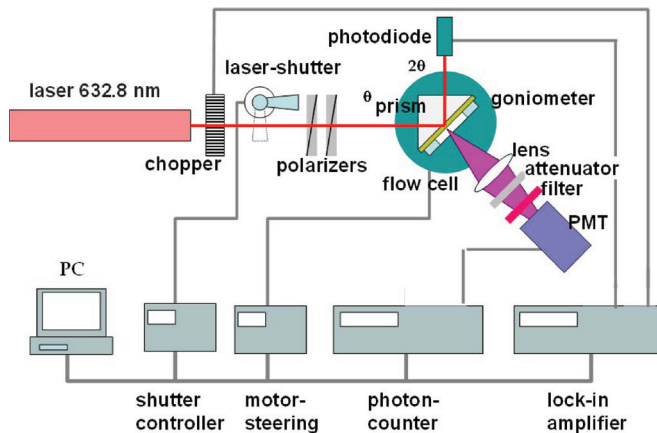


Figure 5.2 Extension of a Kretschmann surface plasmon spectrometer by a fluorescence detection unit consisting of a collection lens, an attenuator (if needed), a set of filters for the separation of scattered light, and a photomultiplier tube (PMT) or a (color) CCD camera for the microscopic mode of operation.

the momentum between the incoming laser photons and the evanescent surface plasmon modes. As one scans the angle of incidence in the normal angular $\theta/2\theta$ scan mode, an attached detection module rotates together with the prism collecting the emitted fluorescence photons through a spectral filter that differentiates the fluorescence from elastically scattered laser light. Typically, the detector is a photomultiplier or an avalanche photodiode but can be replaced in the imaging mode by a color CCD camera that allows then for multiplexed detection of fluorescence from an array of sensor elements in a parallel read-out mode [23].

An example for the sensitivity and LOD achievable with surface plasmon fluorescence spectroscopy (SPFS) is given in Fig. 5.3. The example describes the simplest case of an affinity reaction: The polymer brush was functionalized by the covalent attachment of mouse antibodies to which rabbit anti-mouse antibodies labeled with a fluorescent chromophore could bind. At the given concentrations this binding was purely diffusion controlled: After replacing the pure buffer in the flow-cell by an analyte solution of a given low concentration (in order to avoid depletion of the low analyte concentrations we always worked in a flow mode), the analyte molecules had to cross the unstirred layer from the bulk solution to the binding sites of the brush at the sensor surface by diffusion. According to Fick's law, this mass transfer limited process resulted in a linear increase of the fluorescence intensity with time with a slope which was directly proportional to the bulk concentration of the analyte solution running through the flow cell. This slope when plotted as a function of the bulk concentration of the employed analyte solution gave a calibration curve which could be recorded over almost six orders of magnitude in concentration (hence, in slope) as shown in Fig. 5.3. The intersection of this calibration curve with the 3σ baseline deviation level measured separately as the (fluorescence) stability limit of the set-up and background gives the limit-of-detection for this sensing platform: We obtain a LOD = 500 aM (5×10^{-16} M) [13].

The observed linear increase of the fluorescence intensity with time can be calibrated for the highest concentration against the simultaneously measured label-free signal from normal SPR spectroscopy in terms of how many protein molecules contribute to the observed fluorescence intensity. If extrapolated to the LOD concentration of $c_0 = 500$ aM one finds that the signal (i.e., the

linear intensity increase with time) at this low concentration level originates from 10 antibody molecules that arrive in every minute at the brush matrix landing per every 1 mm^2 of sensor surface area. In other words, SPFS reaches a sensitivity regime close to the single molecule detection level.

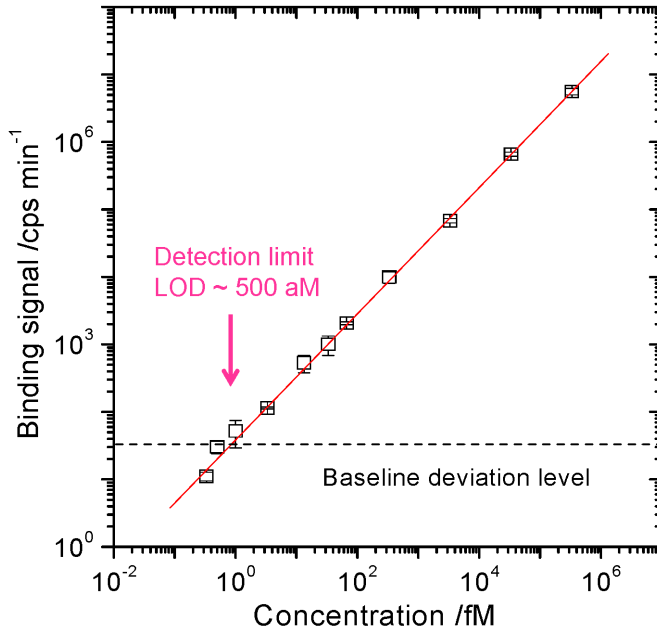


Figure 5.3 Extremely sensitive bio-sensors by SPFS: Shown is a plot of the slopes obtained from the binding kinetics as a function of the corresponding bulk concentration. The intersection of the fit to this calibration curve (red line) with the baseline (background fluorescence level) results in a LOD of 500 aM.

In most cases, the analyte is not directly fluorescently labeled; however, SPFS can still be applied even for the detection of unlabeled analyte molecules with a significant gain in sensitivity if, e.g., a sandwich assay is employed well-known from ELISA assays. The principles of this scheme and the results obtained for a brush modified with a capture antibody against prostate specific antigen (PSA) used in combination with a second fluorescence-labeled detection antibody against PSA are shown in Fig. 5.4 [24]. Irrespective of whether we used a one-step assay, i.e., the detection antibody was pre-incubated with the antigen PSA prior to the

injection into the flow cell, or we employed a two-step assay, in which the PSA running through the flow cell was allowed to bind to the capture antibody for some time and then the fluorescently labeled detection antibody “decorated” the bound analyte, we obtained a LOD of better than 100 fM. This limit was not only 2–3 orders of magnitude lower than the clinically relevant analyte concentration; it was also significantly better than what could be achieved with the classical label-free detection, e.g., by SPR spectroscopy.

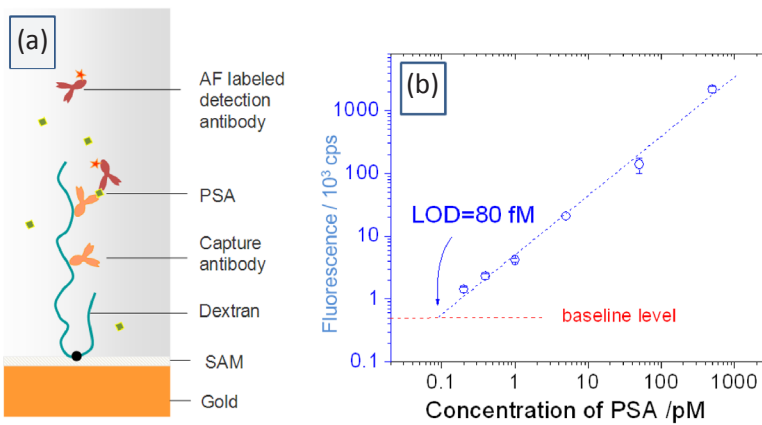


Figure 5.4 (a) Surface architecture of a dextran brush used in an antibody/antigen/antibody sandwich binding assay; (b) calibration curve of the SPFS biosensor for detection of prostate specific antigen.

5.3 Long-Range Surface Plasmon Fluorescence Spectroscopy

If one is dealing with a thin metal film that is sandwiched between two dielectric media of (nearly) identical refractive indices, $n_{b,d}$, plasmon modes excited at each of the two opposite interfaces will interact with each other provided the metal layer is sufficiently thin (thickness d_m of several 10 nm). Then, the optical fields within the metal overlap, which leads to an interaction that lifts off the dispersion degeneracy of the two identical evanescent waves and two new, coupled modes, appear—a symmetrical and an anti-symmetrical wave (referring to their transverse electric

field distribution). The latter one, in particular, has attracted considerable interest because its electric field across the metal film that is responsible for the energy dissipation by the lossy metal is largely reduced and, thus, the propagation length of the mode is considerably increased. Hence, this mode is also called LRSP as opposed to the SRSP mode, which is subject to enhanced dissipation [14].

If we compare some spectroscopic features of regular SPs with those of LRSPs as it is done in Fig. 5.5, we see the following differences: (i) The angular scans of the two types of resonances show a significantly reduced line width that is associated with the excitation of LRSPs compared to that for regular SPs. This is a direct consequence of the reduced dissipation of the energy of the optical field in the metal layer, which is also the reason for the extended propagation length as mentioned before; (ii) if we calculate the field distribution normal to the metal/dielectric interfaces we see a further consequence of the reduced dissipation,

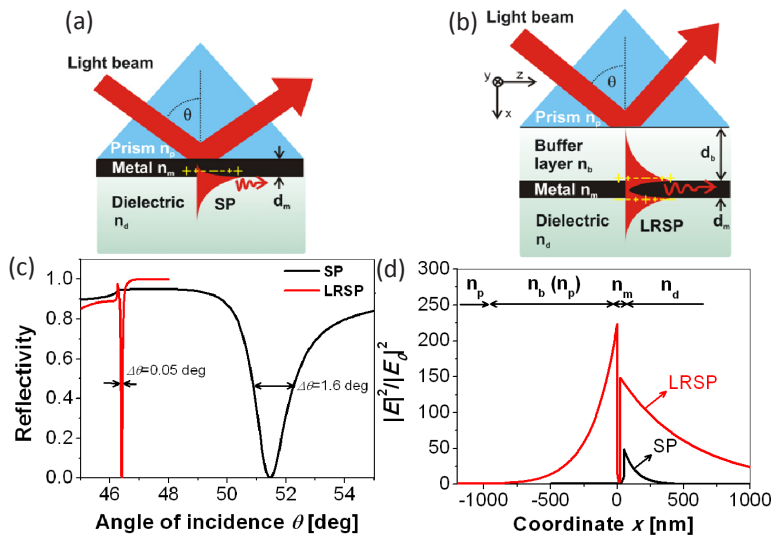


Figure 5.5 Schematic of the ATR coupled with Kretschmann geometry to regular SPs (a) and LRSPs (b). Example of simulated angular reflectivity spectra at the wavelength of $\lambda = 633$ nm and gold films supporting regular SPs ($d_m = 50$ nm) and LRSPs ($d_m = 20$ nm). The gold refractive index $n_m = 0.125 + 3.56i$ was assumed and $n_p = 1.845$, $n_b = 1.310$, $n_d = 1.333$, and $d_b = 850$ nm.

i.e., a significantly enhanced optical field at the interface that also extends into the dielectric media; (iii) and finally, the optical field reaches much farther out into the dielectric. The latter two features are displayed once more in greater detail in Fig. 5.6 where optical field simulations are summarized for LRSPs propagating along gold layers of different thicknesses d_m , ranging from 40 to 15 nm, as indicated. For comparison also the field distribution of normal SPs is shown. One can see that the thinner the metal layer is the higher are the field intensities at the interface metal/dielectric and the farther these fields extend into the dielectric medium.

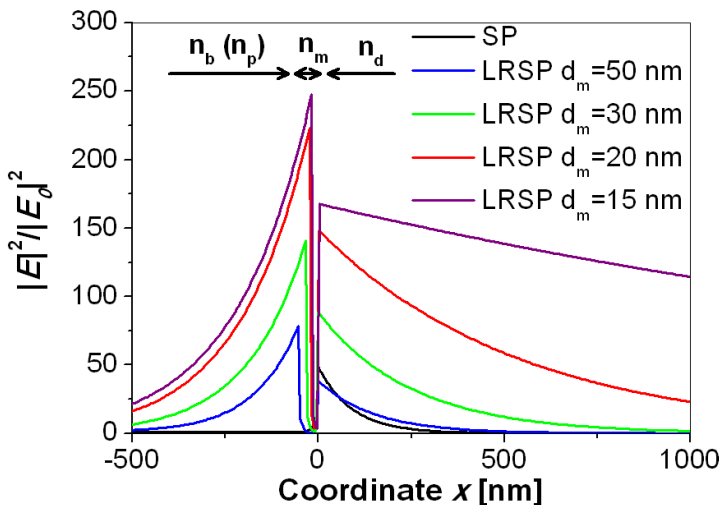


Figure 5.6 Simulated comparison of the field profile of LRSPs propagating along a gold film with varied thickness $d_m = 15, 20, 30,$ and 50 nm. The parameters of layer structures are identical to those used in Fig. 5.5 and the thickness of the buffer layer d_b was adjusted to achieve full coupling to LRSPs.

It was argued [25] that the reduced width of the angular scans of LRSPs would result in a significantly enhanced sensitivity in optical biosensing with surface plasmons: Any thin layer, e.g., a bound protein layer, would result in a much stronger change of the reflected intensity at a given angle of observation because of the higher slope in the reflectivity scan. However, this argument does not take into account the larger extend of the optical field of LRSP modes that can reach out into the dielectric some few μm

(cf. Fig. 5.6). In the overall refractive index architecture seen by the propagating LRSP wave an adsorbed protein layer changes the refractive index from $n = 1.33$ to about $n = 1.45$ of only a very thin slice of a few nm in thickness which has only a minor impact on the dispersion of LRSP modes. As a consequence, the shift of the resonance curve induced by this protein layer probed by LRSPs, hence, is largely reduced compared to regular SPR with the much stronger confinement of optical field of a normal surface plasmon mode nearer to the metal/dielectric interface. However, for fluorescence spectroscopy with LSRPs only the enhanced optical field is relevant and counts towards the obtainable sensitivity increase as we will demonstrate below [15]. As one can see in Fig. 5.6, this intensity enhancement is significant only for the very thinnest metal layers and, hence, the question arises as to whether one can actually prepare metal films in this thickness range that would allow for the translation of this field enhancement into a sensitivity increase in biosensing.

Furthermore, the experimental realization of the general concept of LRSP excitation requires an interfacial architecture that offers for surface plasmon modes propagation along the two interfaces of an ultrathin metal layer in contact with two dielectric media their nearly identical refractive index. In biosensing one of these dielectric media will be water or buffer with a refractive index close to $n_d = 1.33$. Hence, the material of the opposite (proximal) side of the metal layer needs to be a material that (i) has an equivalently low refractive index and that (ii) can be prepared in a way that in can be coated with the thin metal layer, typically by evaporation (cf. also the comparison of the two architectures for SPR and LRSP excitation given in Fig. 5.5). The materials of choice are two commercially available fluorine containing polymers, one called Teflon AF and the other Cytop; both have a refractive index near that of water ($n_b = 1.31$ for Teflon AF and $n_b = 1.34$ for Cytop at the wavelength of $\lambda = 633$ nm), both can be prepared in the required thickness range of typically up to 1 μm , and both are sufficiently smooth at their surface and are well suited for the evaporation of the ultrathin metal layer in the required thickness range. This is demonstrated in Fig. 5.7 where AFM images demonstrate the bare polymer support (a), and the metal layers with nominal thicknesses of the Au films of $d_{\text{Au}} = 30$ nm (a), 22.5 nm (b), and 15.8 nm (c), respectively.

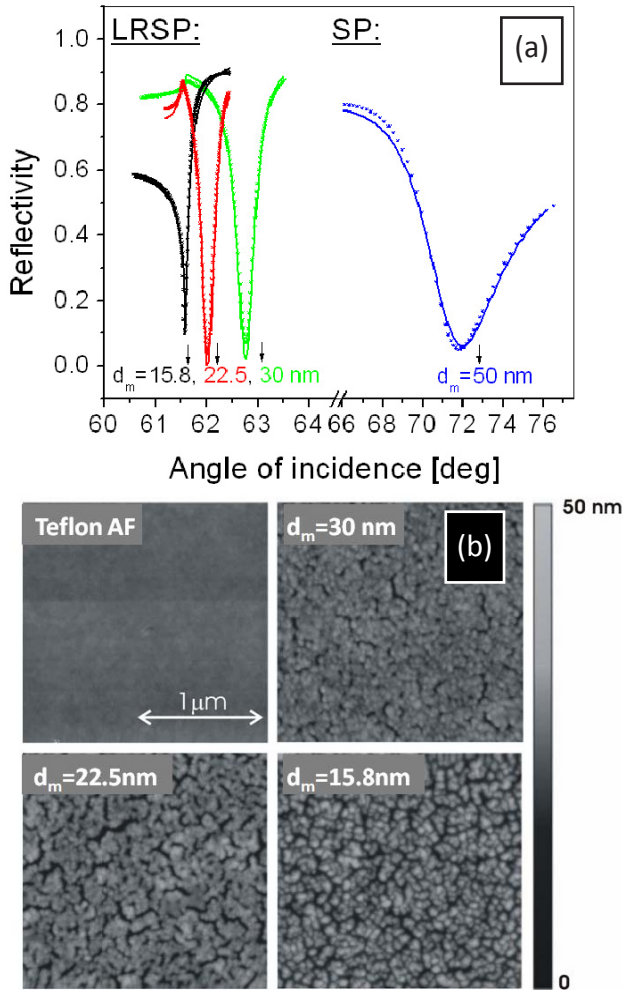


Figure 5.7 (a) Angular reflectivity and (b) morphology of gold films supporting LRSPs. The thickness of gold films d_m between Teflon AF and water was varied as indicated in the graphs.

Shown are further the angular reflectivity scans for the excitation of the LRSP modes in these three thin Au layers taken after having been brought into contact with water. For comparison, also the angular scan of a regular SPR experiment is displayed. The full curves given and fits to the experimental data with complex refractive index of the Au film ($n_m = n'_m + i \cdot n''_m$) revealed that n_m is almost identical for that of bulk Au for the

thickness $d_m > 25$ nm [26]. However, below this thickness island morphology of gold film on fluoropolymers with low surface energy become pronounced which leads to the enhanced damping of LRSPs and decreased field intensity enhancement $|E|^2/|E_0|^2$. This problem can be overcome by chemical modification or plasma treatment of surfaces of fluoropolymer layers [27, 28].

A first demonstration of the obtainable fluorescence intensity increase and, hence, sensitivity enhancement is given in Fig. 5.8. Compared are the angular reflectivity scans for regular SPR in the Kretschmann prism-coupling mode and for a slightly modified layered sample architecture that allows for LRSP excitation. Furthermore, the simultaneously recorded angular scans of the fluorescence intensities are given for both, SPR and LRSP excitation, respectively. In order to demonstrate specifically the significant gain in fluorescence intensities measured for LRSP as a consequence of both, the higher optical field and the longer decay length into the dielectric, we chose a model sample architecture

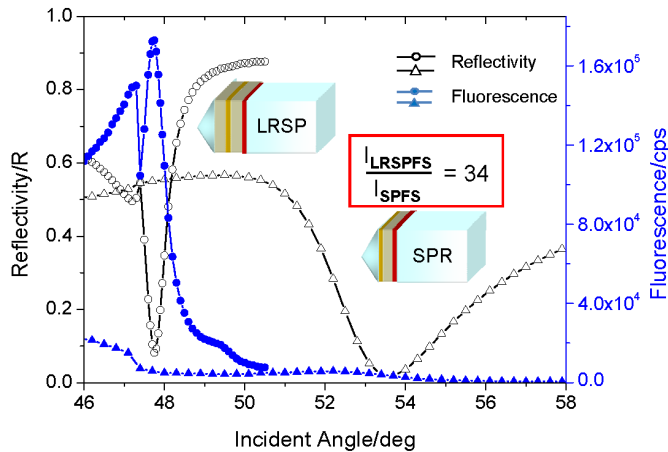


Figure 5.8 Comparison of the angular reflectivity scans recorded with normal SPR (open triangles) and in the LRSP configuration (open circles), together with the simultaneously measured angular fluorescence intensity curves (full triangles for SPFS and full circles for the LRSP fluorescence, respectively). The sample consisted of the prism, a 500 nm-thick cladding layer in the case of the LRSP excitation, an Au layer of 40 nm in each case, a 500 nm Teflon coating on top of the Au in both cases, and the chromophore labeled protein layer adsorbed from solution.

that allowed us to position the fluorescent chromophore layer some 500 nm away from the surface of the Au layer. For SPFS, with its exponential decay of the optical intensity at a decay length of about 90 nm only, this distance to the Au/dielectric interface results in a very weak excitation field and, hence, rather low level of fluorescence emitted by the chromophores (cf. Fig. 5.8, open black and blue full triangles). However, as expected (cf. the simulations in Fig. 5.6) the fluorescence intensity at resonant excitation of a LRSP wave was still significant, with a peak intensity ratio $I_{\text{LRSPFS}}/I_{\text{SPFS}} = 34$ [15]. This can be directly translated into a gain in sensitivity for biosensing applications [29–31].

5.4 Optical Waveguide Fluorescence Spectroscopy

Rather than going into more details of LRSPFS and giving more examples for its use in monitoring bioaffinity reactions we turn our attention to another version of surface wave enhanced biosensing, which is again a direct extension of the platforms discussed so far, i.e., guided optical waves, or (optical) waveguides for short [17]. The basic structural feature of an interfacial architecture that is able to guide light is schematically given in Fig. 5.9: On top of the metal layer that couples the laser photons in the total internal reflection mode of the Kretschmann prism setup and that is functionalized for biosensing applications by a hydrogel that carries the binding sites for the bioaffinity reactions with the analyte molecule from solution [19], new optical modes appear in the reflectivity scan. These modes are guided within the hydrogel layer provided this matrix layer has a refractive index, n_h , slightly higher than that of the adjacent buffer medium, n_d , and is sufficiently thick to ensure that the mode equation for guiding light in this slab waveguide format is fulfilled [32]:

$$\tan(\kappa d_h) = \frac{\gamma_d n_h^2 / \kappa n_d^2 + \gamma_m n_h^2 / \kappa n_m^2}{1 - (\gamma_d n_h^2 / \kappa n_d^2)(\gamma_m n_h^2 / \kappa n_m^2)}. \quad (5.1)$$

This equation holds for transversal magnetic polarization (TM) and β is the propagation constant of guided modes, n_m states for the refractive index of the substrate, and d_h is a thickness of

the hydrogel film. Terms $\kappa^2 = (k_0^2 n_h^2 - \beta^2)$, $\gamma_m^2 = \beta^2 - k_0^2 n_m^2$ and $\gamma_d^2 = \beta^2 - k_0^2 n_d^2$ are the transverse propagation constants in the polymer film, the metal, and the liquid, respectively. For the asymmetric configuration that is characteristic for this type of biosensor format with the metal as the substrate, a hydrogel layer with a thickness in the swollen state of a few μm , a segment density profile typical for soft polymer cushions at interfaces [33], and a refractive index just a little larger than that of the superstrate, i.e., the analyte solution, typically a few guided optical modes can be observed (very schematically shown and indexed in Fig. 5.9 as TM_1 and TM_2). Other than in the case of SP or LRSP modes with their optical field intensities being maximum at the metal surface and then decaying exponentially into the analyte matrix/solution here the optical architecture of the multilayer can be tuned in such a way that a maximum of the optical field is guided nearly completely inside the sensor matrix. This means that the density profile of the fluorescently labeled analytes (or of the fluorescent detection antibodies, cf. the sandwich assay in Fig. 5.4) bound to the capture sites within the hydrogel matrix have a maximum overlap with the probing optical field. Together with the high field enhancement factors that operate inside the waveguide layer this in turn leads to a further significant enhancement of the achievable sensitivity for biosensing applications.

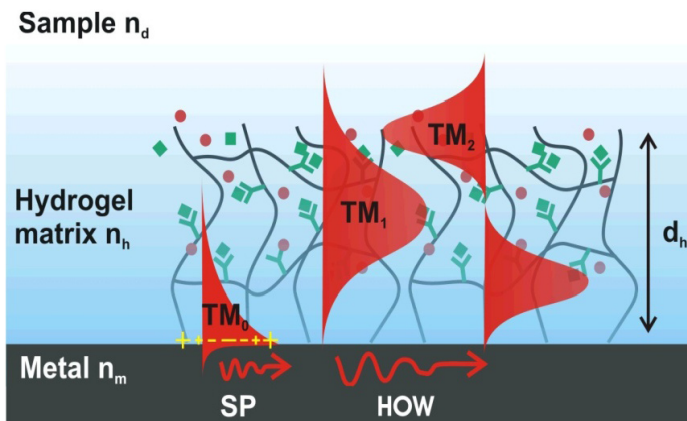


Figure 5.9 Schematics of a hydrogel film attached to a surface of a metal and supported surface plasmon (SP) and hydrogel optical waveguide (HOW) modes for transverse magnetic (TM) polarization.

An example of the two types of fluorescence spectroscopic modes, or more precisely, the two different optical field profiles normal to the waveguide layer are displayed in Fig. 5.10 for a LRSP-supporting layer structure and a hydrogel film with a thickness of $d_h = 1.8 \mu\text{m}$ on the top. One can see that the optical intensity enhancement for the waveguide mode by far exceeds the one for the long-range surface plasmon mode. Furthermore, the field distribution can be tuned in order to probe molecular binding event at specific slice of the hydrogel structure. Both effects lead to the already mentioned higher sensitivity that can be achieved with hydrogel optical waveguide (HOW) spectroscopy as is shown below.

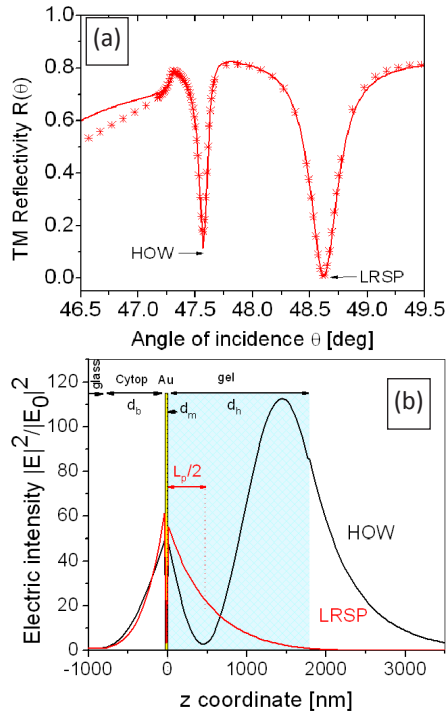


Figure 5.10 Example of (a) angular reflectivity with LRSP and HOW resonances and (b) respective profiles of electric field intensity upon the resonant coupling to these modes. The layer structure consists of a glass substrate with 715 nm-thick Cypot layer, 13.2 nm-thick gold film, and a NIPAAm-based hydrogel with a thickness of $d_h = 1.8 \mu\text{m}$ that is swollen in phosphate buffered saline.

Figure 5.11 documents the implementation of LRSP and HOW modes for the amplified fluorescence immunoassay [21]. In this experiment, a mouse IgG was immobilized on a pNIPAAm-based hydrogel film that simultaneously served as a waveguide and a binding matrix. Afterwards, series of phosphate buffered saline samples spiked with Alexa Fluore 647-labeled anti-mouse IgG were successively flowed over the surface and a fluorescence signal associated with the affinity binding inside the matrix was measured. A comparison of obtained calibration curves for hydrogels films of different thicknesses ($d_h = 0.06, 0.36,$ and $1.8 \mu\text{m}$, as indicated) and fluorescence excitation via LRSP are presented. These results are compared with those obtained for the probing of the interface with the thickest hydrogel ($d_h = 1.8 \mu\text{m}$) by HOW mode.

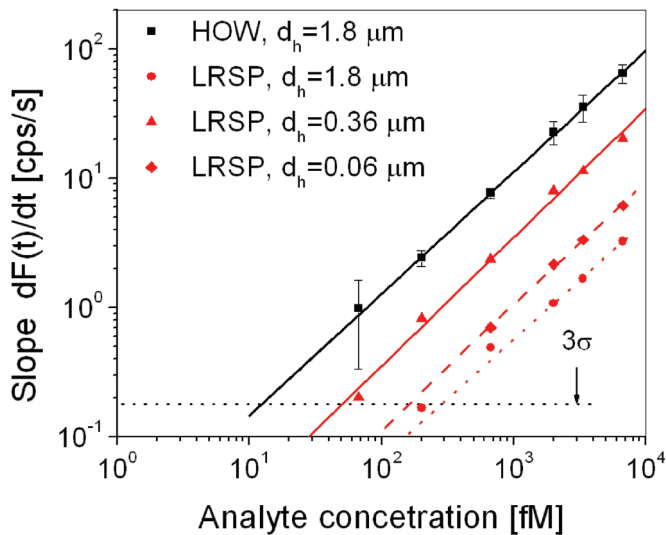


Figure 5.11 Calibration curves measured for the fluorescence immunoassay in a pNIPAAm hydrogel matrix with a thickness of $d_h = 0.06, 0.36$ and $1.8 \mu\text{m}$. The assay utilized Alexa Fluor 647 labels that were excited at the wavelength 633 nm by resonantly excited LRSP and HOW modes as indicated in the graph.

The experimental data were all taken at analyte concentration regimes where mass-transfer limited diffusion leads to a linear increase with time of the fluorescence intensity F after injection

of the analyte solution into the flow cell (cf. also Fig. 5.3). Again, plotting the slopes of these curves dF/dt as a function of the corresponding bulk concentration results in calibration curves that intersect with the background stability limit (3σ) giving the LOD of the corresponding experiment. As one can see in Fig. 5.11 that, indeed, the LOD for HOW is almost an order of magnitude lower than that for the LRSPFS results. However, the interpretation of those data needs a more detailed discussion in order to understand the thickness dependence seen in the data. Far from equilibrium, the affinity binding of target analyte occurs preferably in a top slice of the hydrogel matrix with a finite thickness d_p . This penetration depth d_p depends on a number of parameters. Firstly, it decreases with increasing density of catcher molecules that are attached to the hydrogel matrix as the time the analyte can diffuse before getting captured is shorten. Secondly, it increases when increasing the diffusion coefficient of the analyte in the polymer networks as it allows travel farther into the gel within the time required for the capture. Let us note that for hydrogel matrices typically used in our laboratory, d_p typically reaches several 100 nm. Therefore, for the probing of the hydrogel binding matrix with LRSP modes the highest sensitivity is achieved when $d_h \sim d_p$ (which occurred for $d_h = 0.36 \mu\text{m}$ in the example shown in Fig. 5.11). For larger thicknesses d_h , the sensitivity decreases as the affinity binding events occur outside the LRSPs evanescent field (see Fig. 5.10b). However, almost 10-fold increased sensitivity can be achieved for the detection scheme that utilizes HOW mode supported by a thicker hydrogel layers with $d_h = 1.8 \mu\text{m}$. The reason is that the excitation of these modes is associated with higher field intensity enhancement that is stronger confined at the top slice of hydrogel matrix where the target molecules preferably bind.

5.5 Conclusions

The race for the most sensitive platform for biosensing applications is not decided yet (and certainly will not be for a long period of time): Optical concepts compete with electronic read-out ideas and vice versa. Among the various actively pursued principles in the optical regime surface plasmon excitations play a prominent and promising role, either as the currently very fashionable

electromagnetic resonances localized in different types of (noble) metal nanostructures (particles, shells, other nano-objects with more complex shapes (triangles, cubes, stars) and strings and/or arrays thereof) or in various formats involving propagating modes, typically bound to a metal/dielectric interface.

In this short review, we focused on the latter case of surface-bound electromagnetic waves that can be also used as the light source for the excitation of chromophores thus allowing for the development of sensor concepts that combine the field enhancement mechanisms of surface plasmon excitation with the intrinsic sensitivity of fluorescence spectroscopy. We demonstrated that this way, unprecedented sensitivities could be reached, e.g., for the monitoring of affinity binding reactions of (fluorophore-labeled) analytes of interest with their surface-immobilized receptor structures (demonstrated for the case of an antigen-antibody interaction) which led to the (limit of) detection of 5×10^{-16} M, corresponding to the quantitative detection of only a few protein molecules per mm^2 reaching the sensor surface in every minute.

Extending this concept of combining the field enhancements achievable at resonant excitation of surface plasmon modes with fluorescence detection principles to the use of long-range surface plasmon waves with their strongly enhanced optical fields (due to their strongly reduced interaction with the lossy metal layer resulting in largely de-damped modes) resulted in even higher fluorescence signals of the bound analytes. This was not only a consequence of the mentioned field enhancement; this could be also achieved by making use of the much higher penetration length of the LRSP mode into the analyte solution: By coupling the binding sites to the polymeric backbone of a grafted hydrogel layer we could use both the higher field strength and the larger penetration depth to further enhance the sensor signal recorded for long-range surface plasmon-enhanced fluorescence spectroscopy compared to those obtained when using regular surface plasmons as the excitation light source.

From there, it was only a minor step to explore other modes of excitation that can be observed in surface grafted hydrogels of sufficient thickness: Optical modes guided within the hydrogel layer with an optical field (distribution) that corresponds not only to an exponentially decaying profile with the maximum intensity at the metal-sensor layer interface but rather can exhibit an

intensity distribution that covers the whole thickness of the sensor layer slice (in the μm range). This way, an even higher fraction of the guided modes are actually propagating within the sensor matrix resulting in a further enhancement of the fluorescence signal of the analyte molecules.

Optical detection principles based on propagating surface plasmon waves (but not limited to those) continue to challenge the world of electrical/electronic/electrochemical techniques—the race goes on....

Acknowledgment

This work was only possible through the competent and enthusiastic collaboration of many colleagues. Thanks are due, in particular, to Patrick Beines, Ulrich Jonas, Torsten Liebermann, Bernhard Menges, Thomas Neumann, Hueyoug Park, Benno Rothenhäusler, Fang Yu, Danfeng Yao, and Manfred Zizlsperger. This work was partially supported by the Austrian NANO Initiative (FFG and BMVIT) through the NILPlasmonics project within the NILAustria cluster (www.NILAustria.at) and by the Austrian Science Fund (FWF) through the project ACTIPLAS (P 244920-N20).

References

1. Liedberg, B., Nylander, C., and Lundstrom, I. (1983). Surface plasmon resonance for gas detection and biosensing, *Sens. Actuator.*, **4**, 299–304.
2. www.biacore.com. [cited].
3. See the special issue of *Plasmonics* that summarizes contributions to a Symposium held in Singapore, November 5–7, commemorating 30 years of SPR in **biosensing**.
4. Knoll, W. (1998). Interfaces and thin films as seen by bound electromagnetic waves, *Ann. Rev. Phys. Chem.*, **49**, 569–638.
5. Yu, F., and Knoll, W. (2004). Immunosensor with self-referencing based on surface plasmon diffraction, *Anal. Chem.*, **76**, 1971–1975.
6. Yu, F., Tian, S., Yao, D., and Knoll, W. (2004). Surface plasmon enhanced diffraction for label-free biosensing, *Anal. Chem.*, **76**, 3530–3535.
7. Yu, F., and Knoll, W. (2005). Surface plasmon diffraction biosensor, *J. Opt. Phys. Mater.*, **14**, 149–160.

8. Rothenhäusler, B., and Knoll, W. (1988). Surface-plasmon microscopy, *Nature*, **332**, 615–617.
9. Hickel, W., Kamp, D., and Knoll, W. (1989). Surface-plasmon microscopy, *Nature*, **339**, 186–190.
10. Zizlsperger, M., and Knoll, W. (1998). Multispot parallel on-line monitoring of interfacial binding reactions by surface plasmon microscopy, *Progr. Coll. Polym. Sci.*, **109**, 244–253.
11. Liebermann, T., and Knoll, W. (2000). Surface-plasmon field-enhanced fluorescence spectroscopy, *Coll. Surf. A*, **171**, 115–130.
12. Neumann, T., Johansson, M. L., Kambhampati, D., and Knoll, W. (2002). Surface-plasmon fluorescence spectroscopy, *Adv. Funct. Mater.*, **12**, 575–586.
13. Yu, F., Persson, B., Lofas, S., and Knoll, W. (2004). Attomolar sensitivity in bioassays based on surface plasmon fluorescence spectroscopy, *Am. Chem. Soc.*, **126**, 8902–8903.
14. Sarid, D. (1981). Long-range surface-plasma waves on very thin metal films, *Phys. Rev. Lett.*, **47**, 1927–1930.
15. Kasry, A., and Knoll, W. (2006). Long range surface plasmon fluorescence spectroscopy, *Appl. Phys. Lett.*, **89**, 101106.
16. Toma, K., Dostalek, J., and Knoll, W. (2011). Long range surface plasmon-coupled emission for biosensor applications, *Opt. Express*, **19**, 11090–11099.
17. Knoll, W. (1997). Guided wave optics for the characterization of polymeric thin films and interfaces, in *Handbook of Optical Properties Vol. II: Optics of Small Particles, Interfaces, and Surfaces* (Hummel, R. E., and Wißmann, P. ed).
18. Wang, Y., Huang, C. J., Jonas, U., Wei, T., Dostalek, J., and Knoll, W. (2010). Biosensor based on hydrogel optical waveguide spectroscopy, *Biosens. Bioelectron.*, **25**, 1663–1668.
19. Aulasevich, A., Roskamp, R. F., Jonas, U., Menges, B., Dostalek, J., and Knoll, W. (2009). Optical waveguide spectroscopy for the investigation of protein-functionalized hydrogel films, *Macromol. Rapid Commun.*, **30**, 872–877.
20. Raccis, R., Roskamp, R., Hopp, I., Menges, B., Koynov, K., Jonas, U., Knoll, W., Butt, H., and Fytas, G. (2011). Probing mobility and structural inhomogeneities in grafted hydrogel films by fluorescence correlation spectroscopy, *Soft Matter*, **7**, 7042–7053.

21. Huang, C. J., Dostalek, J., and Knoll, W. (2010). Long range surface plasmon and hydrogel optical waveguide field-enhanced fluorescence biosensor with 3D hydrogel binding matrix: On the role of diffusion mass transfer, *Biosens. Bioelectron.*, **26**, 1425–1431.
22. Knoll, W., Kasry, A., Liu, J., Neumann, T., Niu, L., Park, H., Robelek, R., and Yu, F. (2008). Surface plasmon fluorescence techniques for bio-affinity studies, in *Handbook of Surface Plasmon Resonance* (Schasfoort, R. B. M., and Tudos, A. J., ed.), p. 275–312.
23. Liebermann, T., and Knoll, W. (2003). Parallel multispot detection of target hybridization to surface-bound probe oligonucleotides of different base mismatch by surface-plasmon field-enhanced fluorescence microscopy, *Langmuir*, **19**, 1567–1572.
24. Yu, F., Persson, B., Lofas, S., and Knoll, W. (2004). Surface plasmon fluorescence immunoassay of free prostate-specific antigen in human plasma at the femtomolar level, *Anal. Chem.*, **76**, 6765–6770.
25. Wark, A. W., Lee, H. J. and Corn, R. M. (2005). Long-range surface plasmon resonance imaging for bioaffinity sensors, *Anal. Chem.*, **77**, 3904–3907.
26. Dostalek, J., Kasry, A., and Knoll, W. (2007). Long range surface plasmons for observation of biomolecular binding events at metallic surfaces, *Plasmonics*, **2**, 97–106.
27. Huang, C. J., Dostalek, J., and Knoll, W. (2010). Optimization of layer structure supporting long range surface plasmons for surface plasmon-enhanced fluorescence spectroscopy biosensors, *J. Vac. Soc. Technol. B*, **28**, 66–72.
28. Mejjard, R., Dostalek, J., Huang, C. J., Griesser, H., and Thierry, B. (2013). Tunable and robust long range surface plasmon resonance for biosensor applications, *Opt. Mater.*, **35**, 2507–2513.
29. Wang, Y., Dostalek, J., and Knoll, W. (2009). Biosensor for detection of aflatoxin M₁ in milk based on long range surface plasmon enhanced fluorescence spectroscopy, *Biosens. Bioelectron.*, **24**, 2264–2267.
30. Wang, Y., Brunsen, A., Jonas, U., Dostalek, J., and Knoll, W. (2009). Prostate specific antigen biosensor based on long range surface plasmon-enhanced fluorescence spectroscopy and dextran hydrogel binding matrix, *Anal. Chem.*, **81**, 9625–9632.
31. Huang, C. J., Sessitsch, A., Dostalek, J., and Knoll, W. (2011). Long range surface plasmon-enhanced fluorescence spectroscopy biosensor for ultrasensitive detection of *E. coli* O157:H7, *Anal. Chem.*, **83**, 674–677.

32. Dostalek, J., and Knoll, W. (2012). Plasmonics, in *Polymer Science: A Comprehensive Reference* (Matyjaszewski, K., and Möller, M., ed.), Elsevier: Amsterdam. p. 647–659.
33. Beines, P.W., Klosterkamp, I., Menges, B., Jonas, U., and Knoll, W. (2007). Responsive thin hydrogel layers from photocrosslinkable poly(*N*-isopropylacrylamide) terpolymers. *Langmuir*, **23**, 2231–2238.